

Solute effect of Cu on interdiffusion in  $\text{Al}_3\text{Ti}$  compound films

J. Tardy\* and K. N. Tu

*IBM Thomas J. Watson Research Center, Yorktown Heights, New York 10598*

(Received 3 October 1984)

We study the interdiffusion and formation of  $\text{Al}_3\text{Ti}$ , in bimetallic thin films of Al/Ti and (Al—0.25 at. % Cu)/Ti, both with and without W diffusion markers, in the temperature range 350–500°C. The growth kinetics of  $\text{Al}_3\text{Ti}$  and marker displacement were measured by Rutherford backscattering spectroscopy. Complementary structural and compositional information were obtained by glancing-incidence x-ray diffraction, transmission electron microscopy, Auger-electron spectroscopy, and secondary-ion-mass spectroscopy. The effect of Cu, revealed by marker analysis of the intrinsic diffusivities of Al and Ti in  $\text{Al}_3\text{Ti}$ , is to increase the activation energy of Ti diffusion from 1.68 eV to 2.17 eV while the diffusion of Al is much less affected. By examining the crystal structure of  $\text{Al}_3\text{Ti}$ , a vacancy mechanism with Cu occupying Al sites is proposed to explain the solute effect.

## I. INTRODUCTION

The use of Al metallization in microelectronic Si devices has encountered two severe problems; one is electromigration<sup>1</sup> along interconnecting lines and the other is Al penetration<sup>2</sup> through contact areas. Electromigration leads to line openings and can be resisted by adding a few percent of Cu to the Al. This solution will become inadequate in future devices of smaller dimensions. Consequently, the formation of an intermetallic compound in the sandwich structure of Al/Ti/Al has been studied for further improvement of resisting electromigration.<sup>3</sup> The penetration produces pits which short the underlying junction, so silicide contacts such as PtSi were developed to replace the Al contact. However, Al reacts rapidly with silicides at relatively low temperatures (300 to 400°C), hence a diffusion barrier must be interposed between them in order to prevent their reaction. Ti-based diffusion barriers such as TiN,<sup>4,5</sup>  $\text{Ti}_{30}\text{W}_{70}$  alloy,<sup>6</sup> or even pure Ti,<sup>7</sup> have been developed for this purpose. In the layered structure Al/Ti/Pd<sub>2</sub>Si, the Ti has been reported<sup>6</sup> to be an effective diffusion barrier upon annealing to 400°C. From a technological viewpoint, it is crucial to understand the reaction between Al and Ti. Since the Al line contains Cu, the effect of Cu on the reaction between Al and Ti is relevant.

Interfacial reaction between Al and Ti has been shown to form the intermetallic compound  $\text{Al}_3\text{Ti}$ .<sup>6</sup> The compound grows alone and obeys diffusion-controlled kinetics. In such a "single-phase" growth, it is possible to carry out marker analysis to unravel the intrinsic diffusivities of Al and Ti in the  $\text{Al}_3\text{Ti}$  compound, which are the key kinetic parameters needed in estimating the rate of Al penetration through the barrier layer. Since no suitable isotope of Al exists and electron spectroscopic techniques are unable to measure the self-diffusion of Al and Ti in  $\text{Al}_3\text{Ti}$ , marker-motion analysis is presently the only method available for self-diffusion study of the compound.

Very recent works have given evidence for the dramatic effect of Cu contamination of reactions in Al/Ti,<sup>8,9</sup> Al/W,<sup>8</sup> and Al/Hf (Ref. 9) bimetallic thin films. For every case Cu (in the few percent range) was shown to slow down the reaction kinetics. No conclusive explanation has yet been given and the exact role of copper still remains unanswered.

In this paper, we report measurements of the growth kinetics of  $\text{Al}_3\text{Ti}$  from 350 to 500°C in thin film couples of Al/Ti and (Al—0.25 at. % Cu)/Ti. A noncontinuous film of W (10 Å thick) was used as a diffusion marker in both sets of films. We have observed the effect of Cu on slowing down the interdiffusion process even at such a low concentration. The determination of the temperature dependence of the intrinsic diffusivities of Al and Ti in  $\text{Al}_3\text{Ti}$  shows that the effect of Cu is much greater on Ti diffusion than on Al diffusion in  $\text{Al}_3\text{Ti}$ . The role of Cu is explained on the basis of Cu atoms occupying Al sites in the compound.

## II. EXPERIMENTAL

The substrates used in this study were (111)-oriented silicon wafers covered with a 5000-Å-thick thermally grown oxide. Following the standard cleaning procedure, i.e., brushing with a detergent, ultrasonic cleaning, rinsing in deionized water and drying, they were loaded in the evaporation chamber which was evacuated by an oil diffusion pump. Backstreaming of hydrocarbons was avoided by using an optically blind water-cooled baffle on top of the diffusion pump, and a liquid-nitrogen trap fitted with a titanium sublimator was used to reduce the presence of water vapor and residual oxygen. Furthermore a second liquid-nitrogen shroud and Ti sublimator set-up was mounted at the top of the chamber close to the substrate to further improve the cleanliness of the vacuum. Just before deposition, Ti was evaporated as a getter for oxygen. The pressure was less than  $1 \times 10^{-7}$  Torr before evaporation and rose to  $1.5\text{--}4 \times 10^{-7}$  Torr during eva-

poration. A film of Ti was deposited first to a thickness of 2000 Å at a rate of 20–30 Å/s. Then half of the samples were masked and on the other half, a thin layer (10 Å) of W was deposited at a very low rate (2 Å/s). Finally the shutter was open again and 2000 Å Al or (Al–0.25 at. % Cu) alloy films were deposited at a rate of 20–30 Å/s. Thus, in this process the films were stacked under vacuum without much elapsed time between successive evaporations. The substrates were kept near room temperature during all the depositions.

The as-deposited samples were then isothermally annealed at temperatures ranging from 350 to 500°C for periods between 10 min and 20 h in a quartz tube furnace flushed with helium gas purified by passing through a Ti bed held at 900°C. The partial pressure of oxygen in the furnace was in the low 10<sup>-9</sup>-Torr range.

The growth kinetics were determined by 2.3-MeV He<sup>+</sup>-ion Rutherford backscattering (RBS). The incoming particles impinged upon the target at a tilt angle of 7° and the detection angle was 170°. The spectra were accumulated up to a total dose of 10 μcb to assure good statistics and the beam intensity was kept at ~30 nA. The thickness of the compound layer was calculated from the spectra by assuming the bulk density and using the surface energy approximation in the energy loss parameter calculation. It will be shown in Sec. IV that the precision on the determination of the intrinsic diffusion coefficients of Ti and Al is related exclusively to the precision of the measured Al<sub>3</sub>Ti layer thickness and to the position of the marker relative to the position of surface W. In the following, the precautions needed in carrying out these measurements will be discussed.

First, the thicknesses of Al<sub>3</sub>Ti layers were determined from the energy separation ΔE between two points taken at the half-height of the Ti in Al<sub>3</sub>Ti and the Ti in Ti peaks, respectively. This apparent thickness is corrected for the "resolution width" ΔE<sub>0</sub>, where ΔE<sub>0</sub> is the energy width calculated in the same way for the as deposited Ti layer, by using a quadratic subtraction. The actual energy width of the Al<sub>3</sub>Ti layer is then ΔE<sub>a</sub> = (ΔE<sup>2</sup> - ΔE<sub>0</sub><sup>2</sup>)<sup>1/2</sup>. This correction results in an ΔE<sub>a</sub> which agrees rather well with the exact value derived from the moments method.<sup>10</sup> Only in the case of very thin Al<sub>3</sub>Ti layers can the thickness be substantially underestimated. In that case a cubic subtraction should be more accurate. However, for films of thicknesses above ~500 Å there is no significant difference between thicknesses determined by either the quadratic or the cubic method.

The second point to emphasize is the position of the marker. The width of the W peak in the as-deposited film is very narrow and the peak can be well fitted with a Gaussian distribution, so its centroid is known with an accuracy of tenth of a channel. For annealed samples the W peak is wider but still remains Gaussian in shape, hence its position can also be determined with a very good precision.

Finally, the position of the surface W peak must also be known very accurately. This position is solely dependent on the beam energy which unfortunately varies a little bit from experiment to experiment. From the position of the front edge of the Al surface peak, it is possible to calcu-

late the true beam energy and then to deduce what would be the channel position of a W surface peak. This calibration has been carried out for every set of experimental data.

The composition of the intermetallic phase was determined by RBS and confirmed by glancing-incidence x-ray diffraction. Transmission electron microscopy (TEM) was used to determine the microstructure of the as-deposited films. Auger electron spectroscopy (AES) was carried out on a few samples to determine the amount of oxygen trapped in the films and also the amount of Al dissolved in Ti. Profiling was accomplished in conjunction with 2-keV Ar<sup>+</sup> bombardment. The concentration and distribution of Cu in samples before and after annealing were analyzed by secondary-ion-mass spectroscopy (SIMS).

### III. RESULTS

#### A. Al/Ti and Al/W/Ti systems

##### 1. Microstructure, impurity, and intermetallic compound formation

The microstructure of the films was studied by using transmission-electron microscopy. After chemical etching of the substrate, the samples were ion milled on either the Ti side or the Al side for viewing the Al or Ti, respectively. The Al grain size was about 2000 Å and the dispersion of the grain size was small. The grains contained a low dislocation density and showed a preferred orientation along <111> directions normal to the film surface. The average grain size in the Ti film was about 500 Å and the grains showed a strong <001> preferred orientation normal to the film surface.

The impurity content in the as-deposited films and after annealing for 30 and 225 min at 425°C was analyzed by using AES. The oxygen level in the bulk of the Ti and Al films was below the detection limit of the technique, i.e., <1 at. %. Some oxygen build-up at the Ti-SiO<sub>2</sub> interface was observed; most likely due to the reduction of SiO<sub>2</sub> by Ti during deposition. The build-up extended about 200 Å into the Ti, and moved very little with annealing. In the annealed samples, a rather uniform dissolution of about 4 at. % Al in the unreacted Ti was detected by AES. The dissolution did not increase with annealing time at 425°C, and the amount can be explained by the dissolution of Al along grain boundaries in the Ti film which had a grain size of about 500 Å.

The Cu depth profile in the Al was overly low to be detected by AES. However, the depth profile of Cu in the as-deposited and reacted samples was determined by secondary ion mass spectroscopy (SIMS). The SIMS profiles showed that Cu is uniformly distributed in the as-deposited Al and in the annealed Al<sub>3</sub>Ti samples. No Cu dissolution into Ti nor accumulation in the interfaces could be detected. In Fig. 1 three spectra are shown for the as-deposited films and films annealed at 370°C for 195 min and 450°C for 25 min. The slight increase of the Cu signal for the as deposited films at the Al/Ti interface is insignificant for any change of concentration, but rath-

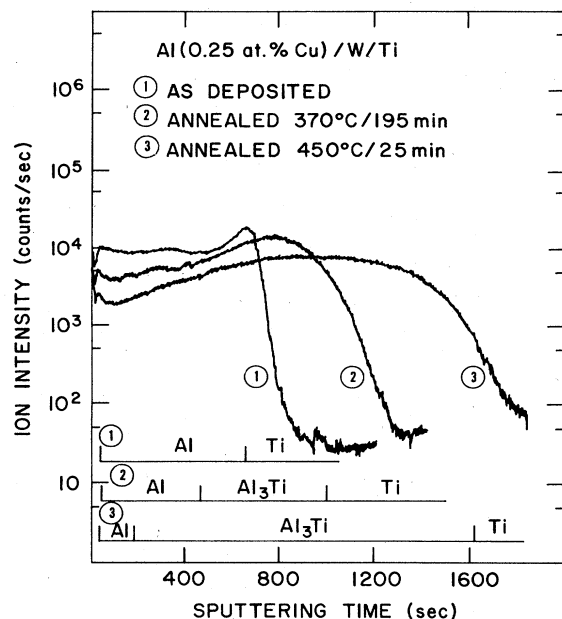


FIG. 1. Cu in depth profiles determined by SIMS for the as-deposited and reacted films. The approximate thicknesses of corresponding layers are represented below the profile. The increase of the Cu signal at the Al/Ti interface for the as-deposited films is probably an artifact due to change of the sputtering yield across the interface.

er, is related to variations in the sputtering yield.

Intermetallic compound formation upon annealing was detected by using glancing-incidence x-ray diffraction. Figure 2 shows the spectra of an Al/Ti sample before and after annealing at 400°C for 90 min. In the temperature range investigated, the one and only intermetallic compound observed was  $\text{Al}_3\text{Ti}$ . We note that a strong (111) reflection of Al and (211) reflection of  $\text{Al}_3\text{Ti}$  can be observed in Figs. 2(a) and 2(b), respectively. The  $\text{Al}_3\text{Ti}$  was found to be stable with excess Ti up to 600°C. When a sample was annealed at 650°C for 1 h, it nevertheless showed the formation of  $\text{Al}_2\text{Ti}$ .

In Fig. 2, an extremely high Ti(103) reflection can be observed. It occurs as a consequence of the strong (001) fiber texture in the Ti film. In the glancing-incidence x-ray diffraction using Seeman-Bohlin geometry and Cu  $K\alpha$  radiation, it is the (103) rather than the (001) reflection which satisfied the Bragg condition. This has been confirmed by calculating the angle between (103) and (001) planes in Ti and by tilting and rotating the sample during diffraction in order to meet or avoid the Bragg condition.

The deposition of W between the Al and Ti does not change the microstructure of the Al film nor the oxygen content. However, it delays the growth of  $\text{Al}_3\text{Ti}$ , as will be discussed in the following.

## 2. Growth kinetics of the $\text{Al}_3\text{Ti}$ compound layer

Figure 3(a) shows Rutherford backscattering spectra (RBS) of the growth of  $\text{Al}_3\text{Ti}$  in the Al/Ti samples an-

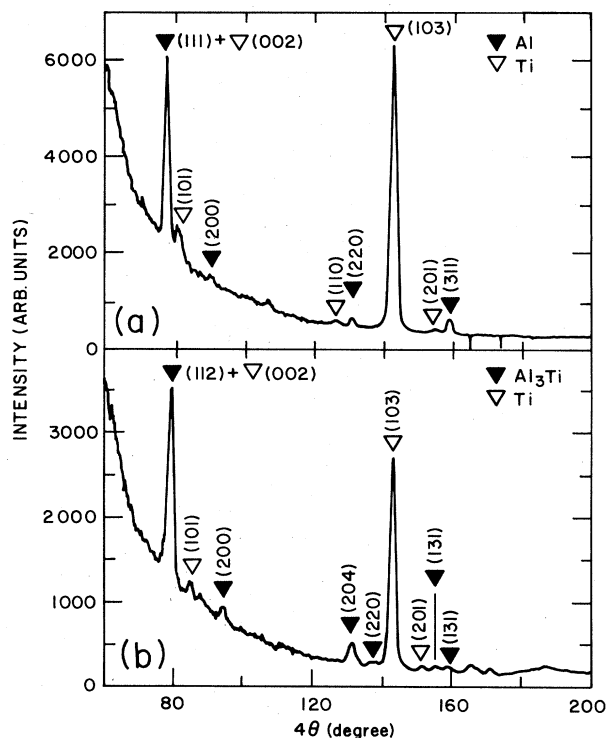


FIG. 2. (a) X-ray diffraction diagram for the as-deposited films and (b) films after annealing at 400°C for 90 min. Only  $\text{Al}_3\text{Ti}$  is observed to form in the range of temperature of annealing we have performed.

nealed at 400°C as a function of time. The evolution of steps on the right-hand side of the Ti peak and the corresponding steps on the left-hand side of the Al peak indicate a layered compound growth. From the height of these steps, the composition ratio of the compound was determined to be  $[\text{Al}]:[\text{Ti}]=3:1$ . Upon the completion of the reaction at 475°C for 100 min, the product consisted of a layer of  $\text{Al}_3\text{Ti}$  (~2600 Å) on a layer of Ti (~1300 Å) containing 4 at. % of Al.

Figure 3(b) shows RBS spectra for Al/W/Ti samples annealed at 400°C. A similar growth of  $\text{Al}_3\text{Ti}$  occurred, nevertheless the growth rate is seen to be retarded by the presence of W. The corresponding displacements of the W peak are shown in Fig. 3(c). The direction of displacement is toward the high-energy side. The measurement of the displacement will be given in Sec. III C.

The thicknesses "x" of the  $\text{Al}_3\text{Ti}$  layer are plotted against the square root of annealing time for different annealing temperatures in Figs. 4(a) and 4(b) for Al/Ti samples without and with W markers, respectively. In Fig. 4, the square root of time dependence indicates diffusion-controlled growth. If we represent the growth by

$$x^2 = 4\tilde{D}_a t, \quad (1)$$

where  $\tilde{D}_a$  is the apparent chemical interdiffusion coefficient in  $\text{Al}_3\text{Ti}$ , an Arrhenius plot of  $\tilde{D}_a$  versus  $1/T$  as shown in Fig. 5 allows the determination of the prefactor  $\tilde{D}_0$  and the activation energy  $Q$ ,

$$\tilde{D}_a = \tilde{D}_0 \exp(-Q/k_B T). \quad (2)$$

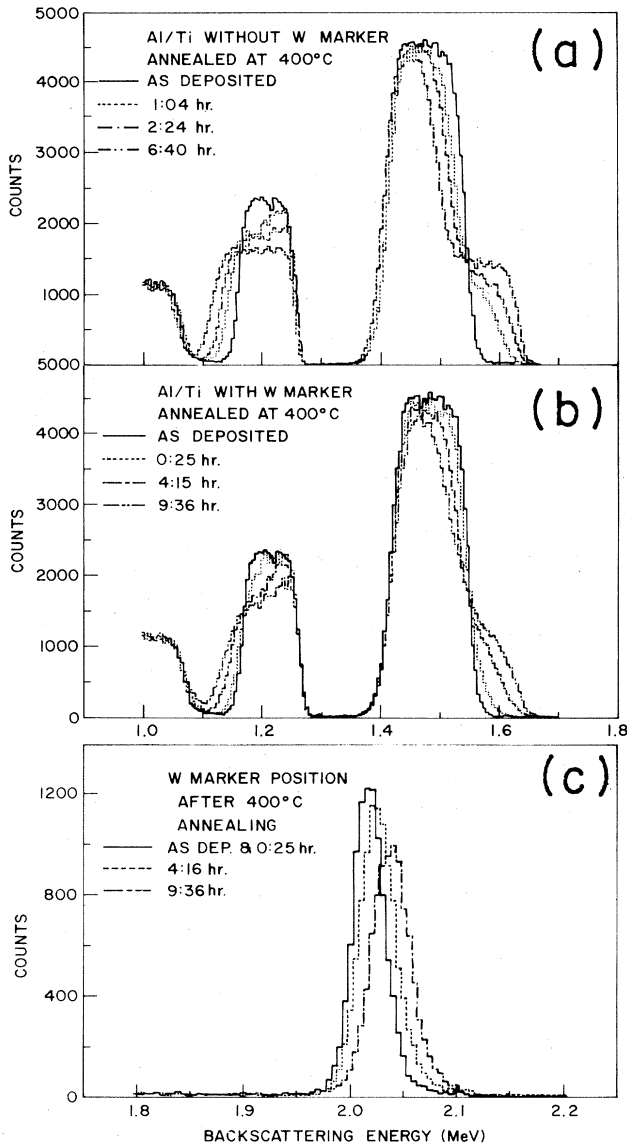


FIG. 3. (a) RBS Spectra for Al-Ti bilayers after different periods of annealing at  $400^\circ\text{C}$ . The conditions are  $2.3\text{ MeV He}^+$  ions impinging at  $7^\circ$  tilt angle, and backscattered ions detected at  $170^\circ$ . (b) RBS spectra for Al/ $10\text{ \AA}$  W/Ti structures. A small slowing down of the  $\text{Al}_3\text{Ti}$  thickening is observed due to the presence of W. (c) High-energy part of Fig. 3(b), where the W peak displacement is shown following heat treatments at  $400^\circ\text{C}$ . The peak is seen to remain narrow and symmetric even after prolonged annealing periods at relatively high temperatures.

For samples without W markers,  $\tilde{D}_0 = 6 \times 10^{-2}\text{ cm}^2/\text{s}$  and  $Q = 1.72 \pm 0.1\text{ eV}$ . For samples with W markers,  $\tilde{D}_0 = 2.5 \times 10^{-2}\text{ cm}^2/\text{s}$  and  $Q = 1.72 \pm 0.1\text{ eV}$ . We note that the W markers reduced  $\tilde{D}_0$  by a factor of 2 to 3, yet the activation energy of growth remains unchanged.

## B. Al(Cu)/Ti and Al(Cu)/W/Ti systems

### 1. Microstructure, impurity, and intermetallic compound formation

Since the concentration of  $0.25\text{ at.}\%$  of Cu in Al is below the solubility limit, no Al-Cu intermetallic com-

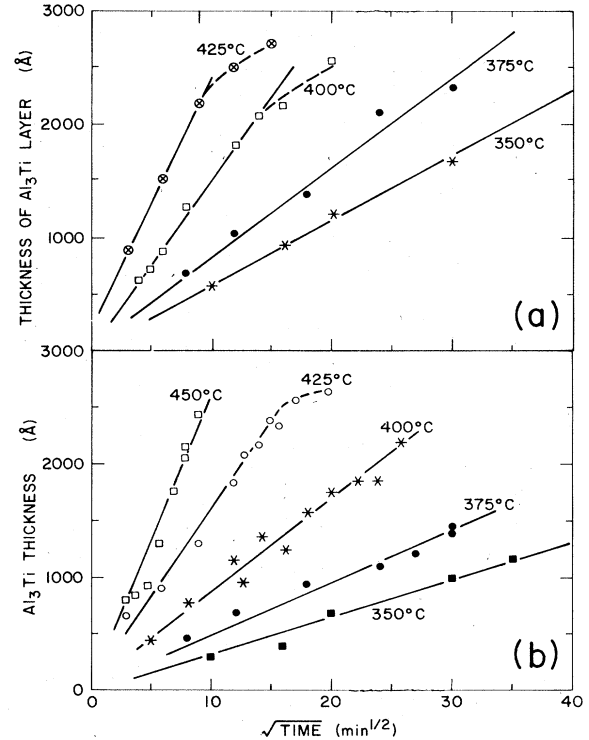


FIG. 4. Time dependence of the thickening of  $\text{Al}_3\text{Ti}$  layer with the temperature as parameter for samples without W marker (a) and with W marker (b). The diffusion governed process is in evidence in both cases.

pound can be detected by electron diffraction or by x-ray diffraction. The microstructure of the Al(Cu) film was similar to the Al film free of Cu. The Auger profiles of the Al(Cu) were the same as those for the Cu-free samples. The oxygen level was below the detection limit of

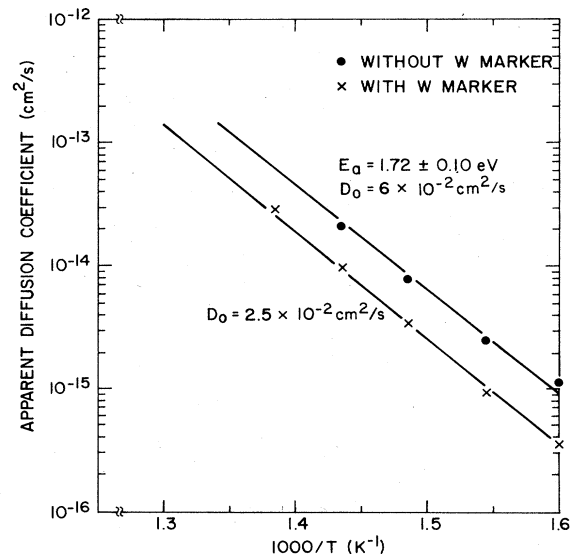


FIG. 5. Arrhenius plot of the apparent diffusion coefficient (kinetic factor). The straight lines are least-square fits to experimental points.

1%, there was a small build-up of oxygen near the Ti-SiO<sub>2</sub> interface, and a dissolution of 4 at. % of Al in the unreacted Ti was again observed. Upon annealing, the only intermetallic compound formation was Al<sub>3</sub>Ti. Neither Al<sub>2</sub>Cu nor any Cu-Ti compounds were detected.

## 2. Growth kinetics of the Al<sub>3</sub>Ti compound layer

Figures 6(a) and 6(b) show RBS spectra for Al(Cu)/Ti and Al(Cu)/W/Ti samples annealed at 400°C for various periods of time. The thickening of Al<sub>3</sub>Ti is drastically slowed down by a factor of about 2 as compared to the spectra of samples without Cu as shown in Figs. 3(a) and 3(b). For example, after an annealing at 400°C for 3 h, the Al<sub>3</sub>Ti thicknesses were 1300 and 2080 Å for

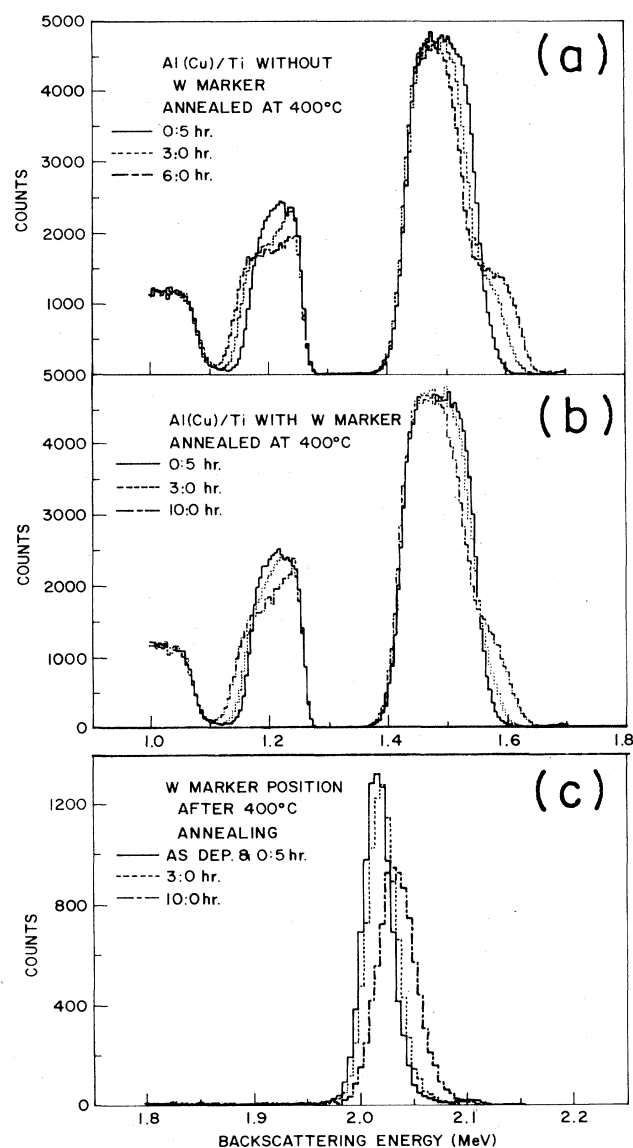


FIG. 6. RBS spectra for (Al-0.25 at. % Cu)/Ti structures recorded in condition identical to the spectra presented on Fig. 3. (a) Samples without W marker. (b) Samples with W marker. (c) Displacement of the W peak upon annealing.

Al(Cu)/Ti and Al/Ti samples, respectively. Figure 6(c) shows marker displacements before and after annealings at 400°C for 30, 180, and 600 min. No displacement was detected before the 30-min annealing. Figures 7(a) and 7(b) show a square-root time dependence for the thicknesses of Al<sub>3</sub>Ti in Al(Cu)/Ti samples without and with W markers, respectively, and Fig. 8 shows the corresponding Arrhenius plots. For samples without W markers,  $\bar{D}_0 = 8 \text{ cm}^2/\text{s}$  and  $Q = 2.05 \pm 0.1 \text{ eV}$ . For samples with W markers,  $\bar{D}_0 = 4 \text{ cm}^2/\text{s}$  and  $Q = 2.05 \pm 0.1 \text{ eV}$ . We note that the effect of adding Cu to Al is to increase the activation energy of interdiffusion by about 0.3 eV and also to increase  $\bar{D}_0$  by two orders of magnitude. Again, the W marker has reduced  $\bar{D}_0$  by a factor of 2.

## C. Measurement of marker positions

In Figure 9, a schematic diagram of a layered growth of Al<sub>3</sub>Ti between Al and Ti is shown, where  $x_1$  is the remaining thickness of Al,  $x_m$  is the marker position measured from the free surface, and  $x_2$  is the total thickness of Al and Al<sub>3</sub>Ti, so the thickness of Al<sub>3</sub>Ti is  $x_2 - x_1$ . Since the accuracy of marker analysis depends critically on the accuracy of measurements of the thickness of Al<sub>3</sub>Ti and the marker position, we shall emphasize below how the measurements of marker position were carried out. We note that the thickness measurement of Al<sub>3</sub>Ti from RBS spectra has been stated in Sec. II.

First, assuming the bulk density for Al ( $\rho = 2.71 \text{ g/cm}^3$ ), Ti ( $\rho = 4.5 \text{ g/cm}^3$ ), and Al<sub>3</sub>Ti ( $\rho = 3.35 \text{ g/cm}^3$ ), we

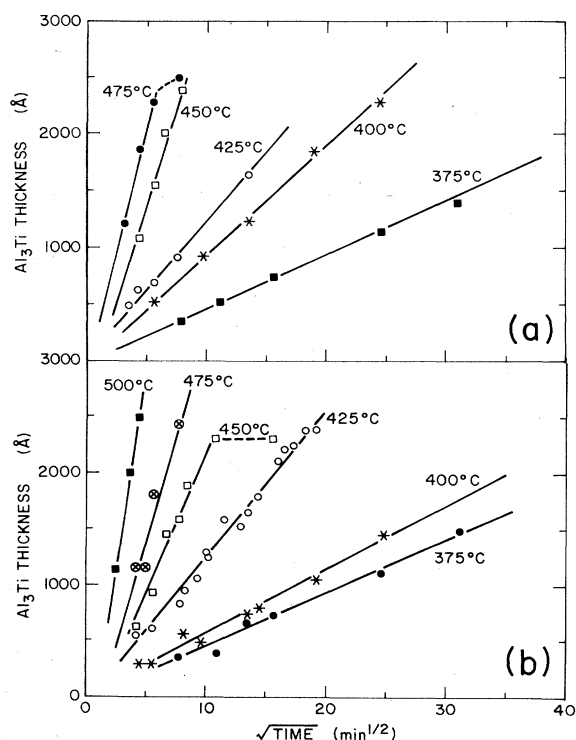


FIG. 7. Time dependence of the thickening of Al<sub>3</sub>Ti layer when 0.25 at. % Cu is added to Al layer for samples without W marker (a) and with W marker (b).

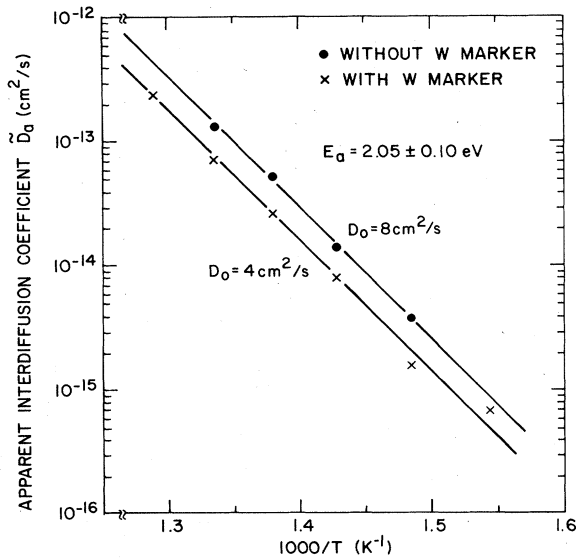


FIG. 8. Arrhenius plot of the apparent diffusion coefficient (kinetic factor). The straight lines are least-square fits to experimental points.

can calculate that the reaction of 1 Å of Al with 0.357 Å of Ti forms 1.33 Å of Al<sub>3</sub>Ti. Therefore, the remaining thickness of Al in units of Å after the formation of  $x$  Å of Al<sub>3</sub>Ti from 2000 Å of Al is deduced from

$$x_1 = 2000 - x/1.33 \quad (3)$$

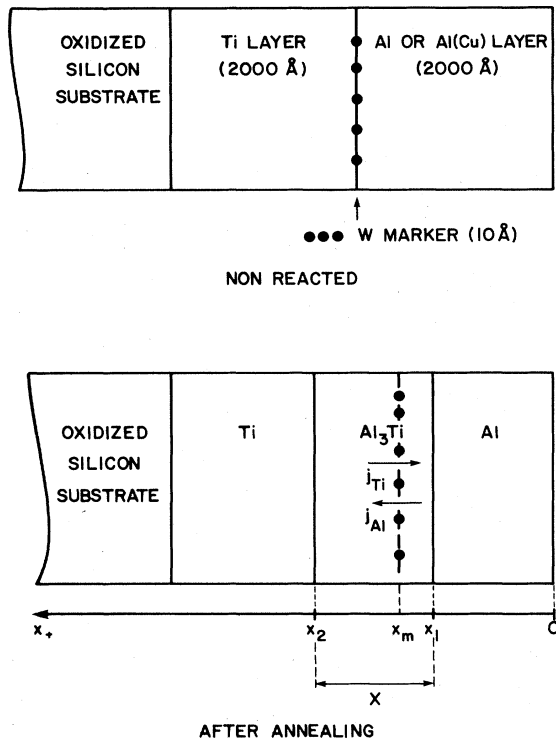


FIG. 9. Cross sectional sketch of the structure nonreacted (top) and after reaction (bottom). The distances  $x_1$ ,  $x_2$ , and  $x_m$  refer to the free surface.

The value of  $x_1$  is needed in determining the marker position  $x_m$ . We have chosen to calculate  $x_1$  from Eq. (3) instead of directly measuring  $x_1$  from the RBS spectra because the latter becomes inaccurate at the beginning (small  $x$  and large  $x_1$ ) and near the end of the reaction (large  $x$  and small  $x_1$ ). In using Eq. (3) to determine  $x_1$ , we have assumed implicitly that all the reacted Al is in Al<sub>3</sub>Ti, in other words there is no other consumption of Al such as the dissolution in Ti. Since we measured (by AES) a dissolution of 4 at. % of Al in Ti, a small correction of the calculated value of  $x_1$  was made accordingly.

To determine  $x_m$ , we note from Fig. 9 that the marker is overlaid with an Al layer of  $x_1$  and an Al<sub>3</sub>Ti layer of  $x_m - x_1$ . Knowing  $x_1$ , it means we have reduced the problem to determining  $x_m - x_1$ .

To proceed, we must first determine the backscattered channel (energy) position " $C_S$ " of a hypothetical W surface layer by the He<sup>+</sup> ion beam. Knowing  $C_S$  and also the energy-loss parameter of He<sup>+</sup> ions in Al, we can determine the backscattered channel position " $C_1$ " of a W marker overlaid by a layer of Al of thickness  $x_1$ . Combining  $C_1$  and the actual backscattered channel position of " $C_m$ " of the W marker and the energy loss parameter of He<sup>+</sup> ions in Al<sub>3</sub>Ti, the value of  $x_m - x_1$  can be determined. The procedure is illustrated in Fig. 10.

In Fig. 10, a straight line is constructed by using the point  $C_S$  and the slope  $S$  (channel/Å of Al) which is the energy loss of backscattered He<sup>+</sup> ions per Å of Al. We have assumed  $S$  to be a constant in the energy range (~2.3 MeV) and the thickness range of Al (<3000 Å) used. Then, a second straight line is constructed by a point  $C_{S1}$  which is below  $C_S$  and a slope  $S'$  (channel/Å of Al<sub>3</sub>Ti). The value of  $C_{S1}$  is the incident ion energy at the

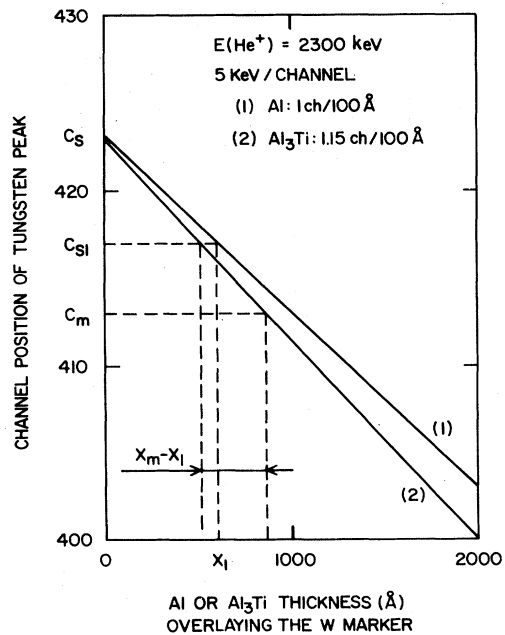


FIG. 10. Graphic method to determine  $x_m - x_1$ , from the knowledge of energy loss of He<sup>+</sup> ions in Al and Al<sub>3</sub>Ti. Calculation presented here are for 2300 keV He<sup>+</sup> and a conversion factor of 5 keV/channel.

$\text{Al}_3\text{Ti}/\text{Al}$  interface and the value of  $S'$  is the energy loss of backscattered  $\text{He}^+$  ions per Å of  $\text{Al}_3\text{Ti}$ . We note that  $C_{S1}$  varies with the thickness of remaining Al, but  $S'$  is again assumed to be a constant. Hence, rather than a single line, we have a set of lines with a constant slope  $S'$ . Now, given  $x_1$  and  $C_m$  and taking an arbitrary value of  $C_{S1}$ , we obtain  $x_m - x_1$  from the two lines as shown in Fig. 9. In short, it is easy to see that

$$x_m = x_1 + (C_S - C_m - x_1 S') / S' \quad (4)$$

We note that in Eq. (4) there is no dependence of  $x_m$  on  $C_{S1}$ , only the slope of the second set of lines is needed. To obtain  $x_m$  as a function of annealing time and temperature, samples were annealed between 360 and 460°C with steps of 10°C. Data of  $x_m$  for samples without and with Cu are plotted against square root of time in Figs. 11(a) and 11(b), respectively. The fact that  $x_m$  is linearly dependent on the square root of the time supports the conclusion that the reaction is diffusion controlled.

#### D. Interfacial drag effect on marker displacement

Marker displacement in the beginning of the reaction may be affected by interfacial drag.<sup>11</sup> A correction for the drag effect must be included in the marker analysis since the marker is assumed to be inert. The marker can be dragged by either one of the two interfaces if the conditions are energetically and kinetically favorable. Breakaway from drag occurs when the motion of the marker cannot keep up with the interface. In Fig. 12, we illustrate the drag effect by assuming that markers are dragged by the  $\text{Al}_3\text{Ti}/\text{Al}$  interface. It is clear that in the as-deposited state as shown in Fig. 12(a) and during the period of drag as shown in Fig. 12(b), we have  $x_m = x_1$ . Then in the period beyond drag as shown in Fig. 12(c), we have  $x_m > x_1$ . To determine when the drag ceases to occur, we replot the data of  $x_m$  together with  $x_1$  and  $x_2$

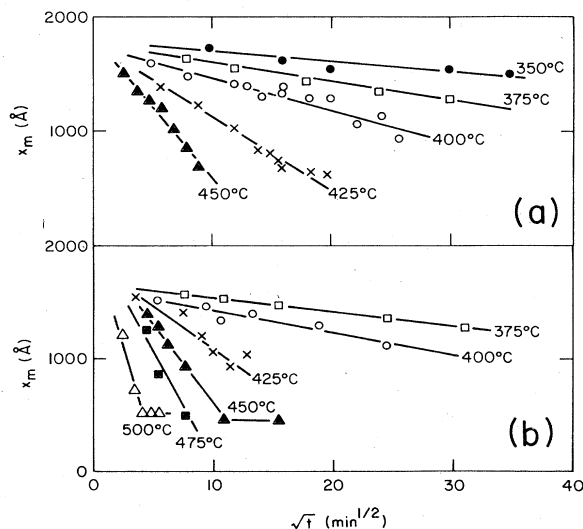


FIG. 11. Time dependence of  $x_m$ , the in-depth position of the W marker for different annealing temperatures: (a) Cu free samples, (b) samples with 0.25 at. % Cu in Al.

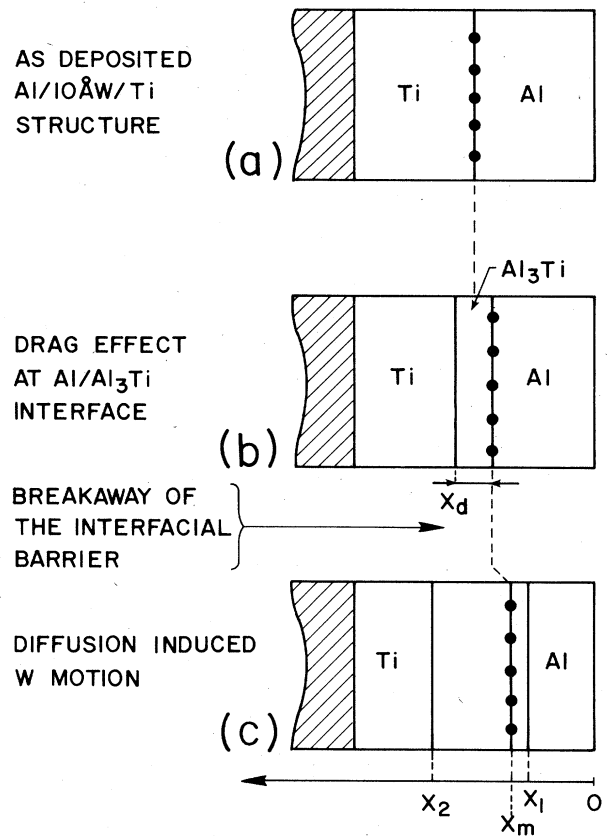
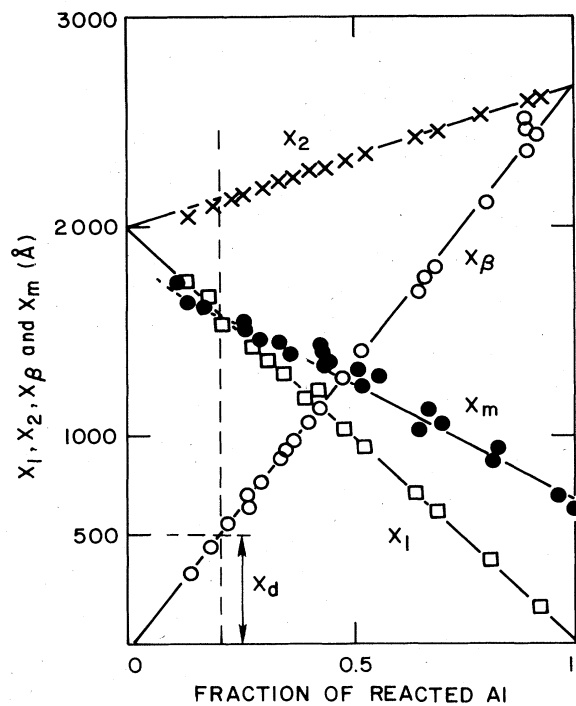


FIG. 12. Schematic representation of the interface drag effect of the marker. From top to bottom: (a) The marker is deposited at the interface of the two metals to interdiffuse and react; (b) during the initial stage the marker is dragged by one of the growing interfaces; (c) after breakaway of the interfacial barrier, the W marker is imbedded in  $\text{Al}_3\text{Ti}$  and its motion can then be related to the diffusion of Al and Ti.

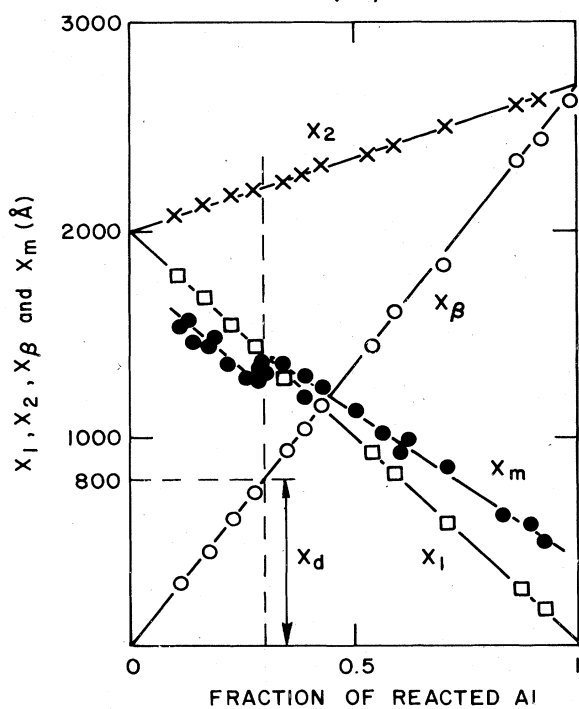
of samples without and with Cu against the fraction of reacted Al (i.e.,  $x_1$  divided by the original thickness of the Al) in Figs. 13(a) and 13(b), respectively. These are linear plots so the temperature dependence of the data is avoided. When the data of  $x_m$  at later stages of reaction is extrapolated linearly back to the beginning of the reaction, the line does not join the lines of  $x_1$  and  $x_2$  at the starting point where ideally we expect  $x_1 = x_m = x_2$ , instead it intercepts the line of  $x_1$ , which is due to interfacial drag of the W markers by the  $\text{Al}_3\text{Ti}/\text{Al}$  interface. We define the point of intercept to be the point where drag is over and the corresponding distance of  $x_2 - x_1$  to be the amount of drag  $x_d$  which must be subtracted from  $x_2$  in the marker analysis of intrinsic diffusivities of  $\text{Al}_3\text{Ti}$  to be given in the next section. We note that the amount of drag and whether it is dragged by the  $\text{Al}_3\text{Ti}/\text{Al}$  or the  $\text{Ti}/\text{Al}_3\text{Ti}$  interface have to be determined by extrapolation.

#### E. Analysis of marker motion

The layered growth of  $\text{Al}_3\text{Ti}$  between Al and Ti has been shown to be diffusion limited. In such a case, there are two unknowns; they are the intrinsic diffusivity of Al



(a)



(b)

FIG. 13. Evaluation of the drag effect magnitude by measuring the minimum thickness of  $\text{Al}_3\text{Ti}$  during the growth of which the marker is linked to the Al- $\text{Al}_3\text{Ti}$  interface: (a) Cu free samples, (b) samples with 0.25 at. % Cu in Al film.

and Ti in  $\text{Al}_3\text{Ti}$ . To determine them, we need to make two independent measurements. Typically, the first one is to measure the thickness of  $\text{Al}_3\text{Ti}$  as a function of time

and temperature and to assume in the following equation [Eq. (1)],

$$x^2 = 4\tilde{D}_a t, \quad (1)$$

that  $\tilde{D}_a$  is equivalent to the chemical interdiffusion coefficient so we can express

$$\tilde{D}_a = D_A^\beta / (\beta + 1) + \beta D_B^\beta / (\beta + 1), \quad (5)$$

where  $D_A^\beta$  and  $D_B^\beta$  are the intrinsic diffusivities of Al and Ti in  $\text{Al}_3\text{Ti}$ , respectively and  $\beta$  is the number of A (Al) atoms per B (Ti) atom in the compound  $A_\beta B$  ( $\text{Al}_3\text{Ti}$ ) as shown in Fig. 9. The second one is to place an inert marker within the diffusion couple and measure its position or velocity as a function of time and temperature. The analysis of marker motion for a diffusion-limited layer growth of a single intermetallic compound, has been published.<sup>12</sup> The analysis shows that it is convenient to measure the marker position relative to the two interfaces of the compound in order to obtain the flux ratio,

$$R = \int_0^t |j_A| dt' / \int_0^t |j_B| dt' \\ = \frac{D_A^\beta}{D_B^\beta} = \beta \frac{(x_2 - x_m) - (x_2^0 - x_m^0)}{(x_m - x_1) - (x_m^0 - x_1^0)}, \quad (6)$$

where  $j_A$  and  $j_B$  are the fluxes of A and B in the compound  $A_\beta B$ , and  $x_2^0$ ,  $x_m^0$ , and  $x_1^0$  are the initial positions of  $x_2$ ,  $x_m$ , and  $x_1$ , respectively (see Fig. 9), when there is no interfacial drag. It is clear from Fig. 12 that  $x_2^0 - x_m^0 = x_d$  and  $x_m^0 - x_1^0 = 0$ , so we obtain

$$R = \frac{D_A^\beta}{D_B^\beta} = \frac{\beta(x_2 - x_m - x_d)}{x_m - x_1}. \quad (7)$$

Therefore, by measuring  $\tilde{D}_a$  and  $R$ , we can solve  $D_A^\beta$  and  $D_B^\beta$  by combining Eqs. (5) and (7).

We have illustrated the physical picture of marker analysis in the above. However, the use of Eq. (1) which is based on random-walk kinetics, has not taken into account the driving force of intermetallic compound formation. To include the driving force, we must consider motion of the interfaces of the compound. The thickening rate of  $A_\beta B$  between A and B as shown in Fig. 9 can be given as<sup>13</sup>

$$\frac{dx}{dt} = \sum_i \left[ \frac{j_i}{C_i} \right] = j_A \frac{\Omega}{\beta} + j_B \Omega, \quad (8)$$

where  $\Omega$  is the volume per atom in  $A_\beta B$  and the concentration of A and B in the  $A_\beta B$  layer may be expressed as  $C_A^\beta = \beta/\Omega$  and  $C_B^\beta = 1/\Omega$  and the fluxes

$$j_A = D_A^\beta C_A^\beta \Delta H_\beta / x k_B T, \quad (9)$$

$$j_B = D_B^\beta C_B^\beta \beta \Delta H_\beta / x k_B T, \quad (10)$$

where  $\Delta H_\beta$  is the enthalpy per atom of formation of the compound  $A_\beta B$ . Substituting Eqs. (9) and (10) into (8), and by integration, we obtain

$$x^2 = 2(1 + \beta) \frac{\Delta H_\beta}{k_B T} \tilde{D}_a t, \quad (11)$$

where  $\tilde{D}_a$  is the chemical interdiffusion coefficient as



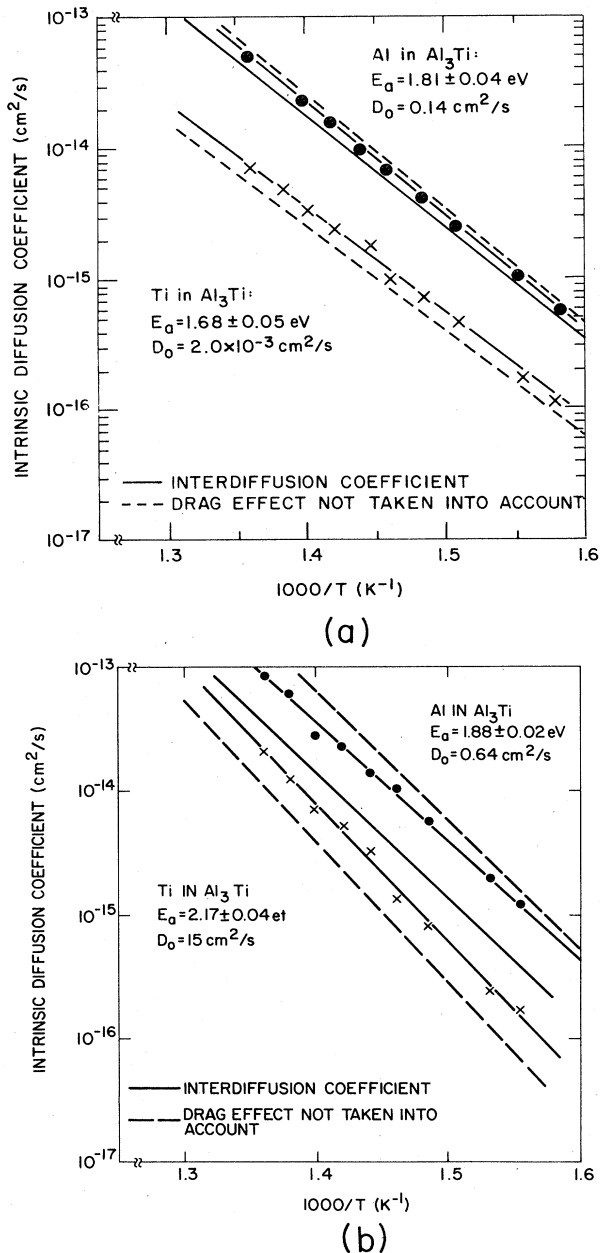


FIG. 14. Intrinsic diffusion coefficients of Al and Ti in  $\text{Al}_3\text{Ti}$ . Also reported are the diffusion coefficient if the drag effect is not taken into account (dashed lines) and the kinetic factor redrawn from Fig. 5 and Fig. 8 for Cu free samples (a) and Cu contaminated samples (b), respectively.

given by Eq. (5). Now combining Eqs. (11), (5), and (7), we have

$$D_B^\beta = \frac{k_B T}{2(R + \beta)\Delta H_\beta} \frac{x^2}{t}, \quad (12)$$

$$D_A^\beta = \frac{Rk_B T}{2(R + \beta)\Delta H_\beta} \frac{x^2}{t}. \quad (13)$$

For the compound  $\text{Al}_3\text{Ti}$ ,  $\beta=3$  and  $\Delta H_\beta=0.38$  eV/molecule.<sup>14</sup> In the calculation of  $D_B^\beta$  and  $D_A^\beta$  from

Eq. (12) and Eq. (13), respectively, the value of  $x$  is the total thickness of the compound layer with correction of  $x_d$ , and the value of  $R$  is also with correction of  $x_d$  as given by Eq. (7).

In Figures 14(a) and 14(b), Arrhenius plots of  $\tilde{D}_a$ ,  $D_{\text{Al}}$ ,  $D_{\text{Ti}}$  versus  $1/T$  for samples without and with Cu, respectively, are shown. Values of activation energies and pre-exponential factors are listed in Tables I and II.

#### IV. DISCUSSION

To use marker analysis in studying the solute effect on interdiffusion, the selection of marker, the determination of marker position and the measurement of interfacial drag are crucial to the accuracy of quantitative analysis and in turn the finding of the true solute effect. The marker has to be inert and detectable; W was selected for these two reasons. The solid solubility of W in Al is less than 0.2 at. % at 715°C and in Ti about 0.25 at. % at 650°C, also W forms intermetallic compounds with Al but not with Ti.<sup>15</sup> It is conceivable that the W marker could react with Al to form compounds and/or dissolve into Al and Ti, yet these reactions were not observed in our experiment since the W peaks in RBS spectra remain relatively sharp and intensive. A possible explanation for no reaction between the Al and W is the moderate annealing temperatures used in the experiment. Because of the large mass difference between W and Al (or Ti), the W peak was isolated in RBS spectra so its position can be accurately determined. The coverage of deposited W on Al surfaces has been shown to be extensive, therefore we deposited W on Ti in order to produce a discontinuous W. However, the W marker was found to slow down the growth of  $\text{Al}_3\text{Ti}$  by a factor of 2 to 3. It is conceivable that a decrease of W thickness may remove the effect of retardation, but the tradeoff is the detectability. Since the activation energies are not affected by the marker, we assume the marker analysis remains valid.

To interpret our results, we first examine the crystal structure of  $\text{Al}_3\text{Ti}$ . Figures 15(a) and 15(b) show, respectively, a schematic crystal structure of Al (two unit cells) and  $\text{Al}_3\text{Ti}$  (one unit cell). A portion of a close-packed  $\text{Al}_3\text{Ti}$  plane, the (112) plane, is illustrated in Fig. 15(b). The crystal structure of  $\text{Al}_3\text{Ti}$  is body-centered tetragonal (bct) with lattice constants  $a=3.84$  Å and  $c=8.61$  Å and there are two lattice sites per unit cell and four atoms (one Ti and three Al) per lattice site.<sup>16,17</sup> For convenience, if we ignore the difference between Al and Ti, we may regard the crystal structure of  $\text{Al}_3\text{Ti}$  as a deformed fcc structure of Al ( $a=4.049$  Å) with an elongation of 6.7% along the  $c$  direction and a contraction of 4.5% in the  $a$  and  $b$  directions. Consequently, diffusion in  $\text{Al}_3\text{Ti}$  lattice is to a first-order approximation close to what happens in a close-packed fcc lattice.

For self-diffusion via vacancy mechanism in fcc metals, there is an empirical rule between the lattice-diffusion activation energies ( $Q$ ) and melting-point ( $T_m$ ),<sup>18,19</sup>

$$\frac{Q}{T_m} = 35 \frac{\text{cal}}{\text{K}}. \quad (14)$$

Let's take Al as an example. Its lattice-diffusion activa-

TABLE I. Diffusion coefficients in Al<sub>3</sub>Ti.

Thin-film structure	Reference No.	Interdiffusion coefficient		Intrinsic diffusion D <sub>0</sub> (cm <sup>2</sup> /s)	coefficient Q (eV)
		D <sub>0</sub> (cm <sup>2</sup> /s)	Q (eV)		
Al/Ti	7	0.15	1.85		
Al/Ti	8	0.2 <sup>a</sup>	1.8 ±0.1		
Al/Ti	9	3.4 × 10 <sup>-3</sup>	1.6		
Al/Ti	This work	6 × 10 <sup>-2</sup>	1.72 ± 0.10		
Al/W/Ti ( < 10 Å W)	This work	2.5 × 10 <sup>-2</sup>	1.72 ± 0.10	Al 0.14 Ti 210 <sup>-3</sup>	1.81 ± 0.04 1.68 ± 0.05

<sup>a</sup>Determined from published figure.

tion energy and melting-point are 1.45 eV and 933 K, respectively, so we have  $Q/T_m = 35.7$  cal/K. In the case of Al<sub>3</sub>Ti, with a measured chemical interdiffusion  $Q = 1.72$  eV and a melting point of 1613 K, we obtain  $Q/T_m = 24.5$  cal/K, so we may not use the relation shown in Eq. (14) to conclude that the measured diffusion coefficients are the lattice-diffusion coefficients of Al<sub>3</sub>Ti. However, Eq. (14) may not be applicable to Al<sub>3</sub>Ti, and there is no published data of lattice diffusion in Al<sub>3</sub>Ti for reference. Since the Al<sub>3</sub>Ti thin film is polycrystalline, grain-boundary diffusion may contribute to mass transport, yet the measured activation energy of about 2 eV is too high to be grain-boundary diffusion for a close-packed material with a melting point of 1613 K. In fact, very little is known about grain boundary diffusion in intermetallic compounds. In the following, we shall assume lattice diffusion via vacancies and consider vacant sites in Ti and Al sublattices in Al<sub>3</sub>Ti.

We first note that the unit cell volume of Al<sub>3</sub>Ti which equals  $3.84 \text{ \AA}^2 \times 8.61 \text{ \AA} = 126.96 \text{ \AA}^3$  is smaller than the volume of two unit cells of Al,  $2 \times 4.049^3 \text{ \AA}^3 = 132.76 \text{ \AA}^3$ . So the structure of Al<sub>3</sub>Ti is somewhat compressed as compared to that of Al. In Al<sub>3</sub>Ti, if we classify atoms according to their nearest-neighbor configuration, there are three types, and Figs. 16(a)–16(c) show, respectively, the nearest-neighbor configuration of a Ti atom and two types of Al atoms (type A and type B) in Al<sub>3</sub>Ti. Figure 16(a) shows that each Ti atom has 12 Al atoms but no Ti atoms as nearest neighbors. Figure 16(b) shows that a type-A Al atom has 4 Ti, 8 type-B Al, and no type-A Al as nearest neighbors. Figure 16(c) shows that a type-B Al atom has 4 Ti, 4 type-B, and 4 type-A Al atoms as nearest neighbors. It is clear that only the type-B Al atoms have a sublattice with same type of atoms as nearest neighbors in Al<sub>3</sub>Ti.

In Fig. 16(a), if we replace the Ti atom by a vacancy, the surrounding 12 Al atoms will relax toward the vacant site because of the compressed structure. Moreover, the vacancy tends not to exchange with one of the surrounding Al atoms because that will result in a cluster of Al atoms in a configuration the same as that in pure Al yet compressed. For these reasons, a vacancy in the Al sublattice, which has four nearest-neighbor Ti atoms as shown in Figs. 16(b) and 16(c), will favor the exchange with Ti atoms rather than Al atoms. Then the next most probable jump of the vacancy which has just exchanged sites with a Ti atom is to exchange back with the Ti, making it a highly correlated jump. In other words, a jump of an Al atom into a vacant Ti site requires a high activation energy. If such a jump is necessary for the transport of Al atoms through Al<sub>3</sub>Ti, the measured activation energy of Al migration should be high. Although we have argued in favor of the exchange of a Ti atom with a neighboring vacancy, we must point out that the exchange leads to disorder in the structure, so there is a slight trade off in energy.

To consider a vacancy in the Al sublattice, we note that there are type-A and type-B sites as shown in Figs. 16(b) and 16(c), respectively. For a Ti atom to exchange with a vacant type-A Al site, it has to jump through a window formed by four Al atoms with an area of  $2.716 \text{ \AA} \times 4.305 \text{ \AA} = 11.69 \text{ \AA}^2$ . For a Ti atom to exchange with a vacant type-B Al site, the window consists of four Al atoms and has an area of  $2.88 \text{ \AA} \times 3.84 \text{ \AA} = 11.07 \text{ \AA}^2$ . Clearly, without a detailed energetic calculation, it is difficult to judge whether a Ti atom would prefer to exchange with a vacant type-A site or a vacant type-B site. However, Ti diffusion jumps which consist of exchanges with type-A vacant sites only do not lead to long-range diffusion unless some Al atoms also jump into vacant Ti sites. This is

TABLE II. Diffusion coefficients in Al<sub>3</sub>Ti containing 0.25 at. % Cu.

Thin-film structure	Reference No.	Interdiffusion coefficient		Intrinsic diffusion coefficient	
		D <sub>0</sub> (cm <sup>2</sup> /s)	Q (eV)	D <sub>0</sub> (cm <sup>2</sup> /s)	Q (eV)
(Al–3 at. % Cu)/Ti	8	<sup>a</sup> 2.5 × 10 <sup>4</sup>	2.4 ± 0.10		
(Al–0.5 at. % Cu)/Ti	9	2.9	2.05 ± 0.10		
(Al–0.25 at. % Cu)/Ti	This work	8	2.05 ± 0.10		
(Al–0.25 at. % Cu)/W/Ti ( < 10 Å W)	This work	4	2.05 ± 0.10	Al 0.64 Ti 15	1.88 ± 0.02 2.17 ± 0.04

<sup>a</sup>Determined from published figure.

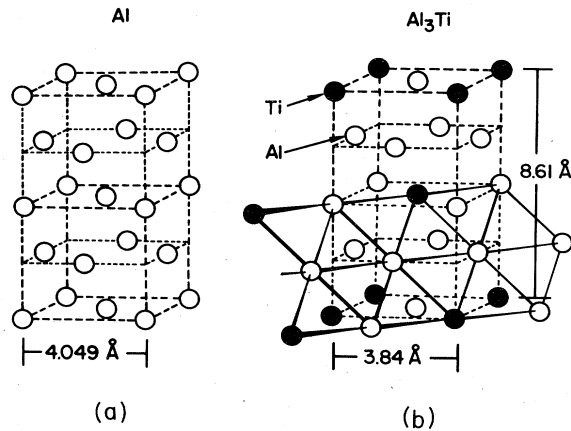


FIG. 15. Schematic representation of two Al fcc unit cells (a) and a  $\text{Al}_3\text{Ti}$  unit cell (b) showing the close structural relationship between the two lattices.

because neither Ti nor type-*A* Al atoms possess nearest neighbors of their own kind. On the other hand, since the type-*B* Al sublattice is continuous, a long-range Ti diffusion can take place via disordered jumps through vacant *B* sites.

Then, we must consider whether a long-range diffusion of Al in  $\text{Al}_3\text{Ti}$  can occur via the *B*-site sublattice, avoiding the Ti sites totally. In principle it could, but we have already pointed out that a vacancy in the Al sublattice always favors the exchange with a Ti atom, so the Al jumps will be interrupted. Thus, to transport Al atoms through  $\text{Al}_3\text{Ti}$ , Al atoms have to make jumps via the vacant Ti sites, which we have already argued will require a high activation energy.

The essence of the above discussion is that a Ti atom is energetically comfortable in the center site shown in Fig. 16(a) because it is the equilibrium structure of  $\text{Al}_3\text{Ti}$ , but not an Al atom because the structure becomes compressed as compared to fcc Al. A vacant Ti site is also energetically favorable because the surrounding Al atoms can relax, therefore vacancies are attracted to the Ti sites. The diffusion of Al atoms, by exchange sites with these vacancies, requires a high activation energy of motion.

The solute effect of Cu shows a large influence on Ti diffusion by increasing its activation energy from 1.67 to 2.17 eV, yet not much on Al diffusion whose activation

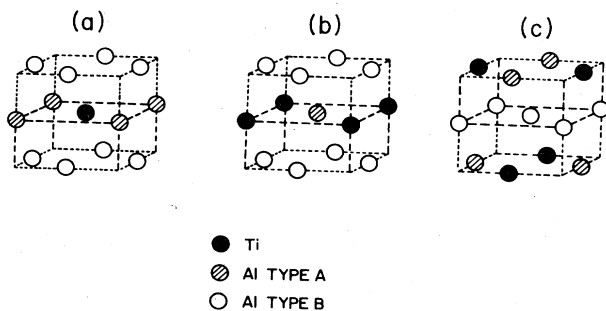


FIG. 16. Details of Fig. 15(b) showing the first neighbor environment for a Ti atom (a), a Al type-*A* atom (b), and a Al type-*B* atom (c).

TABLE III. Thermodynamic data of Al-Cu, Cu-Ti, and Ti-Al compounds.

Alloy <sup>a</sup>	Melting point $T_m$ (K)	Free energy of formation (eV/molecule)	Reference No.
$\text{Al}_2\text{Cu}$	864	0.14	15,14
TiCu	1258	0.2	20
$\text{TiCu}_4$	1158	0.23	20
$\text{Al}_3\text{Ti}$	1613	0.38	15,14

<sup>a</sup>To the best of our knowledge the free energy of formation for  $\text{TiCu}_3$  has not been published so far. Murray (Ref. 20) reported the phase  $\text{TiCu}_3$  is metastable and can be formed before the stable  $\text{TiCu}_4$  structure.

energy change only from 1.81 to 1.89 eV. To understand the effect, it is crucial to determine the relative binding energies among Cu, Ti, and Al atoms, which atomic site in  $\text{Al}_3\text{Ti}$  will Cu occupy, and if there is any influence due to interfacial reaction and segregation.

In Table III, typical free energies of formation of Al-Cu, Cu-Ti, and Al-Ti intermetallic compounds are shown. Generally speaking, formation energies per atom of Cu-Ti and Al-Ti compounds are comparable, and they are higher than those of Al-Cu compounds. This indicates that the binding energy between Cu and Ti is higher than that between Cu and Al.

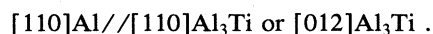
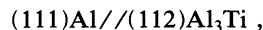
The measured distribution (by SIMS) of Cu in Al before reaction and in Al and  $\text{Al}_3\text{Ti}$  after reaction was very uniform; no accumulation at any interface could be detected. The growth of  $\text{Al}_3\text{Ti}$ , with or without Cu, has been determined to be diffusion controlled, indicating no interfacial effect due to Cu. For these reasons, we conclude that interfacial effect of Cu is negligible.

If we assume Cu to occupy the Ti site as shown in Fig. 16(a), we see that the Cu has no Ti atoms as nearest neighbors, only Al atoms. From the viewpoint of binding energy, this is unfavorable. More significantly, however, the Cu cannot influence Ti diffusion directly since they are not nearest neighbors. Since we observed a big effect of Cu on Ti diffusion, we conclude that Cu solutes dissolve in the Al sublattice and occupy Al sites. Then the questions whether Cu occupies type-*A* or type-*B* site and how does it affect Ti diffusion should be answered.

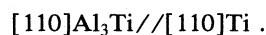
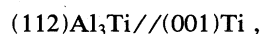
The nominal interatomic distance between a Ti atom and a Cu atom which takes a type-*A* site is 2.716 Å, and the corresponding distance between a Ti atom and a Cu atom which takes a type-*B* site is 2.88 Å. Although the former is closer to one half of the sum of closest approach in pure Cu and pure Ti, an energetic calculation is required in order to distinguish them. Nevertheless, whether a Cu atom jumps from a type-*A* site to a type-*B* site or vice versa, it maintains four Ti atoms as nearest neighbors, so Cu is very effective in tying down Ti atoms. If the binding energy between Cu and Ti in  $\text{Al}_3\text{Ti}$  is strong, it is easy to see from the above picture that the diffusion of Ti will be slowed down and a higher activation energy will be needed in order to break Ti atoms away from Cu atoms. On the other hand, it is also easy to see that Cu has little effect on Al diffusion in  $\text{Al}_3\text{Ti}$  since their binding is weaker than that between Al and Ti.

To summarize the discussion of the effect of Cu on interdiffusion in Al<sub>3</sub>Ti, we have concluded that Cu occupies substitutional sites of Al on the basis of the marker results, the crystal structure of Al<sub>3</sub>Ti, and a stronger binding energy between Cu and Ti atoms.

About the interfaces in the Al/Al<sub>3</sub>Ti/Ti layered structure, it is worth noting that while the misfits between Al and Al<sub>3</sub>Ti across their (100) and (001) planes are quite large as shown in Fig. 16, the misfit between their close-packed planes is less than 1%. This suggests that the following epitaxial relationship could exist between the two:



The strong (111) reflection of Al and (112) reflection of Al<sub>3</sub>Ti as shown in Fig. 2 tend to support the epitaxy. Furthermore, it is also possible to have epitaxy between the basal plane of Ti and the (211) plane of Al<sub>3</sub>Ti. The misfit there is just over 1%. This is easy to see because in close-packed structures, i.e., fcc for Al and hcp for Ti, their closest interatomic distances are 2.862 and 2.89 Å, respectively. Indeed, a strong preferred orientation of (001) of Ti is also found in Fig. 1. Therefore, between Ti and Al<sub>3</sub>Ti we expect



On the basis of the above relations, it is possible to develop a structure of Al/Al<sub>3</sub>Ti/Ti with epitaxy at both interfaces. Such a structure can be prepared by depositing Al and Ti onto glassy or mica surfaces at a high substrate temperature. The low-energy epitaxial interfaces would

enhance the oriented nucleation of Al<sub>3</sub>Ti over other Al-Ti intermetallic compounds between the Al and Ti. Furthermore, the growth of the epitaxial Al<sub>3</sub>Ti when compared to the growth of a fine-grained Al<sub>3</sub>Ti between polycrystalline Al and Ti films can reveal the contribution of grain boundary diffusion in Al<sub>3</sub>Ti to its growth.

Finally, it is conceivable that different solutes may have different effects on Al and Ti interdiffusion. While Cu shows a strong effect on Ti, a transition metal solute might have a bigger effect on retarding Al diffusion. The marker analysis reported here can be used to sort out the details.

## V. CONCLUSIONS

(1) The growth of Al<sub>3</sub>Ti between Al and Ti films is diffusion controlled. Intrinsic diffusivities of Al and Ti in Al<sub>3</sub>Ti are obtained and listed in Table I.

(2) The addition of 0.25 at. % of Cu to Al has greatly retarded the diffusion-controlled growth of Al<sub>3</sub>Ti. The effect of Cu on intrinsic diffusivities is shown in Table II; the most significant finding is the increase of activation energy of Ti diffusion from 1.68 to 2.17 eV.

(3) The effect of Cu on Ti diffusion in Al<sub>3</sub>Ti can be explained by assuming Cu to occupy Al sites and to diffuse via vacancies.

## ACKNOWLEDGMENTS

The authors would like to thank the Central Scientific Service (CSS) Laboratory of the IBM Research Center (Yorktown Heights) for preparing the thin films, P. Saunders for his help in using the Van deGraff accelerator, F. LeGoues for the TEM analysis, J. DeLuca for the SIMS analysis, and R. Shad for the Auger microanalysis.

\*Permanent address: Department de Physique des Materiaux Universite de Lyon, 69621 Villeurbanne, France.

<sup>1</sup>F. M. d'Heurle and P. S. Ho in *Thin Films Interdiffusion and Reaction*, edited by J. M. Poate, K. N. Tu, and J. W. Mayer (Wiley, New York, 1978), Chap. 8.

<sup>2</sup>C. Y. Ting and B. L. Crowder, *J. Electrochem. Soc.* **129**, 2590 (1982).

<sup>3</sup>J. K. Howard, J. F. White, and P. S. Ho, *J. Appl. Phys.* **49**, 4083 (1978).

<sup>4</sup>M. Wittmer, *Appl. Phys. Lett.* **36**, 456 (1980).

<sup>5</sup>M.-A. Nicolet, *Thin Solid Films*, **52**, 415 (1978).

<sup>6</sup>P. B. Ghate, J. C. Blair, C. R. Fuller, and G. E. McGuire, *Thin Solid Films* **53**, 117 (1978).

<sup>7</sup>R. W. Bower, *Appl. Phys. Lett.* **23**, 99 (1973).

<sup>8</sup>I. Krafcsik, J. Gyulai, C. J. Palmström, and J. W. Mayer, *Appl. Phys. Lett.* **43**, 1015 (1983).

<sup>9</sup>H. C. W. Huang and M. Wittmer, *Materials Research Society Symposia Proceedings*, Vol. 25 of *Thin Films and Interfaces*, edited by J. E. E. Baglin, D. R. Campbell and W. K. Chu (North-Holland, New York, 1984), p. 157.

<sup>10</sup>R. F. Lever and W. K. Chu, in *Ion Beam Surface Layer Analysis*, edited by O. Meyer, G. Linker, and F. Käppeler

(Plenum, New York, 1974), p. 149.

<sup>11</sup>K. N. Tu, *J. Appl. Phys.* **48**, 3379 (1977).

<sup>12</sup>U. Gösele, K. N. Tu, and R. D. Thompson, *J. Appl. Phys.* **53**, 8759 (1982).

<sup>13</sup>H. Schmalzried, *Solid State Reactions* (Weinheim, Dearfield Beach, FL, 1981), Chap. 7, p. 147.

<sup>14</sup>R. Hultgen, P. D. Desai, D. T. Hawkins, M. Gleiser, and K. K. Keley, *Selected Values of the Thermodynamical Properties of Binary Alloys* (American Society for Metals, Metal Park, 1973), p. 221.

<sup>15</sup>M. Hansen, *Constitution of Binary Alloys* (MacGraw-Hill, New York, 1958).

<sup>16</sup>W. B. Pearson, *Handbook of Lattice Spacings and Structures of Metals* (Pergamon, Oxford, 1967), Vol. 2.

<sup>17</sup>F. A. Wells, *Structural Inorganic Chemistry*, 3rd ed. (Clarendon, Oxford, 1962).

<sup>18</sup>Y. Adda and J. Philibert, *La Diffusion dans les Solides* (Bibliothèque des Sciences et Techniques Nucleaires, Paris, 1966), Chap. I.

<sup>19</sup>P. G. Shewmon, *Diffusion in Solids* (McGraw-Hill, New York, 1963), p. 65.

<sup>20</sup>J. L. Murray, *Bull. Alloy Phase Diagrams* **4**, 81 (1983).